A Structural and Theoretical Analysis of Transition Metalloporphodimethenes and Their Relationship with Metalloporphyrins

Nazzareno Re,[b] Lucia Bonomo,[a] Carlos Da Silva,[a] Euro Solari,[a] Rosario Scopelliti,[a] and Carlo Floriani*[a]

Abstract: The paper reports the synthesis of the first-row transition metal hexaethylporphodimethene derivatives $[(Et_6N_4)M]$ [M = Mn, **3**; M = Co, **5**; M = Cu, **7**] on a multigram scale, which makes them easily available for reactivity studies. After synthesis they were converted into the corresponding five-coordinate $[(Et_6N_4)M(L)]$ [M = Mn, L = THF, **8**; M = Co, L = Py, **9**] and six-coordinate $[(Et_6N_4)M(L)_2]$ [M = Mn, L = THF, **10**; M = Mn, L = Py, **11**] derivatives. The compounds mentioned above and those recently reported, namely the iron and nickel derivatives **4**, **6**, **12**, and **13**, permit the presentation of the first coherent report on the structural, optical, magnetic, and electronic characteristics of the first-row transition metal porphodimethene derivatives. The experimental results, coupled with a detailed theoretical analysis (Density Functional Theory, DFT), give the appropriate background for future development of the porphodimethene skeleton, which paves the way from porphyrinogen to porphyrins. In addition, this report, encompassing the entire first row of transition metal ion porphodimethenes, allows a valuable comparison to be made with the corresponding metallated porphyrins, thus establishing the peculiar differences in terms of structural and electronic properties and potential reactivity.

Keywords: magnetic properties · metalloporphyrins · porphodimethenes · porphyrinoids

Introduction

Porphodimethenes are very often invoked as the intermediate in the oxidation pathway of porphyrinogen to porphyrins and metalloporphyrins.[1, 2] Studies on such a skeleton, either on the metal-free or the metalated form, are limited by the complicated and small-scale synthetic access.[3] Porphodimethenes can be obtained formally by a two-electron reduction and protonation or alkylation[3] of the porphyrin or by a four-electron oxidation–deprotonation or dealkylation[4] of the porphyrinogen (Scheme 1). The former method, which is limited to sterically hindered octaalkylporphyrins, does not have flexibility in terms of *meso* derivatives and scaling up. The second one, which has been introduced successfully in the literature only recently,[4] has the great advantage of leading to differently *meso*-substituted porphodimethenes and, in addition, can be performed at an appropriate scale for synthetic purposes. Such a synthetic method provides the porphodimethene skeleton in its protonated or lithiated form, the latter being the most appropriate for transmetallation reactions. This is the first comprehensive report on porphodimethene derivatives for the first-row transition metals from Mn^{II} to Cu^{II}. They have been synthesized according to the new methodology, and a structural analysis of the unligated, mono-

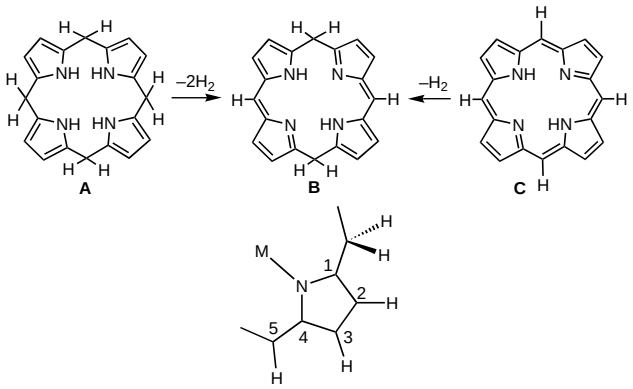

Scheme 1. The two synthetic pathways to the porphodimethene skeleton and the numbering scheme adopted for the porphodimethene ligand.

[a] Prof. Dr. C. Floriani, L. Bonomo, C. Da Silva, Dr. E. Solari, Dr. R. Scopelliti
Institut de Chimie Minérale et Analytique
Université de Lausanne
BCH, 1015 Lausanne (Switzerland)
Fax: (+41) 21-692-39-05
E-mail: carlo.floriani@icma.unil.ch

[b] Prof. N. Re
Facoltà di Farmacia, Università degli Studi G. D'Annunzio
66100 Chieti (Italy)

Supporting information for this article is available on the WWW under http://www.wiley-vch.de/home/chemistry/ or from the author.

 © WILEY-VCH Verlag GmbH, D-69451 Weinheim, 2001 0947-6539/01/0712-2536 $ 17.50+.50/0

and bisligated forms has been completed with a detailed investigation of their magnetic properties.

These results, coupled with a detailed theoretical analysis, give the appropriate background for a perspective on the future development of the chemistry of metalloporphodimethenes. The differences in electronic and structural properties between these two classes of compounds can be particularly important in planning metal-assisted transformations of a variety of substrates.

Results and Discussion

The general synthesis of the *meso*-hexaethylporphodimethene complexes was carried out according to Scheme 2, by treating the THF-solvated metal chlorides with the lithium

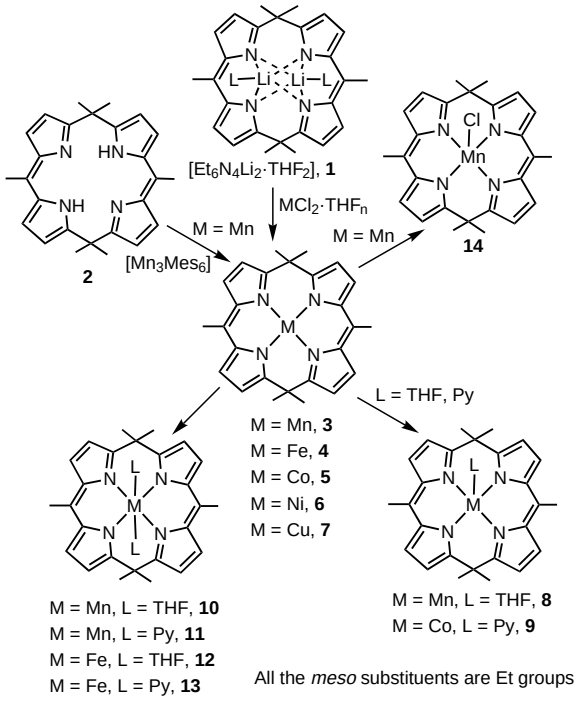

Scheme 2. The synthesis of the tetra-, penta-, and hexacoordinate metallaporphodimethene derivatives.

porphodimethene derivative **1**.[4] The latter was synthesized according to a recently published method.[4] Following the procedures given in the Experimental Section, three forms have been obtained: the base (unligated) chelates **2**–**7**, the monoligated **8** and **9**, and the bisligated **10**–**13**. The detailed results concerning **2**–**13** will be reported and discussed in three different sections: A) *Structural and spectroscopic properties*; B) *Magnetic properties*; C) *Theoretical studies.*

Structural and spectroscopic properties: **Structural analyses** were carried out for the tetracoordinate **5** and **7**, pentacoordinate **8** and **9**, and hexacoordinate **10** and **11**; details are reported in Table 1. For an appropriate structural comparison, we will mention also the structures of **4**, **6**, **12**, and **13**, which we reported recently in a more synthetic context.[4]

The parameters which have been considered and which will be helpful for discussing the relationship with the related metalloporphyrins are: i) the conformational ones summarized in Table 2; ii) the deviation of the metal from the N_4 plane (see Table 2), which depends on the coordination number of the metal and the d^n configuration; iii) the M–N bond lengths, which are reported in Table 3; and iv) the folding of the macrocycles.[4] A major difference from the porphyrin will be, possibly, the size of the cavity of the N_4 core, which may have a different metal selectivity than the porphyrin skeleton (see Table 3). The structures will be considered in groups, depending on the coordination number of the metal, except for **14**, which is the lone M^{III} derivative under consideration.

*Complexes **5** and **7***: Both compounds **5** and **7** (**5** is displayed in Figure 1, while **7** is reported in the Supporting Information) have square-planar coordination geometry and show small

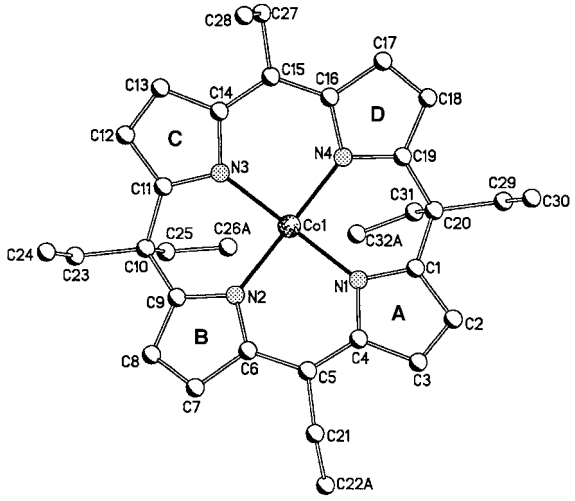

Figure 1. XP drawing of **5** showing the labeling scheme adopted (H atoms and disorder omitted for clarity).

displacements from the N_4 plane [0.022(2) and 0.040(4) Å for **5** and **7**, respectively]. The structural features are similar to those shown in square-planar metal centers bearing this kind of ligand [see Ni^{II} and Fe^{II}], which can be summarized as: i) short M–N bond lengths [$Co–N_{av} = 1.935(3)$ Å, **5**; $Cu–N_{av} = 1.979(8)$ Å, **7**]; ii) roof folding of the ligand with a high degree of ruffling[3f] (see Table 2).

The roof folding (α) can be considered as a measure of the distortion and nonplanarity of the ligand, which is rather flexible compared to porphyrin.[3f] As can be seen from Table 2, the highest value is shown for complex **6**, while, in the case of planar ligands like **12**, this folding is zero. There are some noteworthy intramolecular and intermolecular interactions occurring between CH_2 hydrogens of the ethyl chains and the metal ion ($Co1 \cdots H26B = 2.70$ Å; $Co1 - H32B = 2.70$ Å; $Co1 \cdots H18 = 2.58$ Å).

*Complexes **8** and **9***: These two compounds, shown in Figures 2 and 3, respectively, are very different, even though the metal centers of both have a square-pyramidal arrangement. These

 © WILEY-VCH Verlag GmbH, D-69451 Weinheim, 2001 0947-6539/01/0712-2537 $ 17.50+.50/0

Table 1. Crystal data and details of the structure determination for **5**, **8**, **9**, **10**, **11**, and **14**.

	5	**8**	**9**	**10**	**11**	**14**
Chemical formula	$C_{32}H_{38}CoN_4$	$C_{36}H_{46}MnN_4O$	$C_{37}H_{43}CoN_5$	$C_{40}H_{54}MnN_4O_2$	$C_{42}H_{48}MnN_6$	$C_{32}H_{38}ClMnN_4$
Formula weight	537.59	605.71	616.69	677.81	691.80	569.05
Crystal system	monoclinic	orthorhombic	triclinic	monoclinic	monoclinic	monoclinic
Space group	$P2_1/c$	*Pbca*	$P\bar{1}$	$P2_1/n$	$P2_1/n$	$P2_1/c$
a [Å]	11.5290(9)	14.555(3)	8.7480(17)	10.0283(8)	10.0334(5)	12.542(3)
b [Å]	25.910(2)	17.094(3)	9.5010(19)	10.1986(3)	9.6000(4)	10.231(2)
c [Å]	9.8398(5)	25.760(5)	18.793(4)	17.4789(6)	18.5830(6)	21.914(4)
α [°]	90	90	90.58(3)	90	90	90
β [°]	114.227(6)	90	97.16(3)	92.2350(14)	94.8000(10)	100.42(3)
γ [°]	90	90	96.50(3)	90	90	90
V [Å^3]	2680.4(3)	6409(2)	1539.4(5)	1786.29(16)	1783.65(13)	2765.5(10)
Z	4	8	2	2	2	4
D_{calcd} [g cm^{-3}]	1.332	1.255	1.330	1.260	1.288	1.367
F(000)	1140	2584	654	726	734	1200
μ [mm^{-1}]	0.669	0.446	0.592	0.409	0.409	0.603
T [K]	143	143	143	143	143	143
λ [Å]	0.71073	0.71070	0.71070	0.71069	0.71069	0.71070
Measured reflns	14978	33723	7168	8697	8444	8993
Unique reflns	4455	5300	4182	2619	2375	3628
Unique reflns [$I>2(I)$]	4138	4006	3678	1954	1949	2028
Data/parameters	4455/363	5300/380	4182/389	2619/214	2375/223	3628/344
R[a] [$I>2(I)$]	0.0601	0.0477	0.0476	0.0545	0.0440	0.0757
$wR2$[a] (all data)	0.1268	0.1401	0.1417	0.1371	0.1030	0.2166
GoF[b]	1.144	1.003	1.097	1.127	1.218	0.917

[a] $R=\Sigma||F_o|-|F_c||/\Sigma|F_o|$, $wR2=\{\Sigma[w(F_o^2-F_c^2)^2]/\Sigma[w(F_o^2)^2]\}^{1/2}$. [b] $GoF=\{\Sigma[w(F_o^2-F_c^2)^2]/(n-p)\}^{1/2}$, where n is the number of data and p is the number of parameters refined.

Table 2. Comparison of relevant structural parameters within the metal–ligand units.

		5	**8**	**9**	**10**	**11**	**14**	**6**	**4**	**12**	**13**
Deviations from the N_4 core [Å]	N1	0.022(2)	0.006(1)	−0.008(1)	0	0	−0.063(3)	0.009(2)	0.003(1)	0	−0.014(1)
	N2	−0.022(2)	−0.006(1)	0.008(1)	0	0	0.063(3)	−0.009(2)	−0.003(1)	0	0.014(1)
	N3	0.022(2)	0.006(1)	−0.008(1)	0	0	−0.064(3)	0.009(2)	0.003(1)	0	−0.014(1)
	N4	−0.022(2)	−0.006(1)	0.008(1)	0	0	0.064(3)	−0.009(2)	−0.003(1)	0	0.014(1)
	M	0.022(2)	−0.298(1)	−0.052(2)	0	0	−0.303(3)	0.072(2)	−0.045(1)	0	−0.043(1)
Angle between AB[a] (β1) [°]		26.6(3)	6.2(2)	22.2(2)	3.6(3)	8.6(2)	19.0(4)	16.8(1)	23.2(1)	2.7(1)	15.4(1)
Angle between CD[a] (β2) [°]		24.7(2)	14.9(2)	21.8(1)	3.6(3)	8.6(2)	17.9(4)	24.1(2)	25.2(1)	2.7(1)	19.3(1)
Roof folding[b] (α) [°]		44.4(3)	11.2(2)	52.2(1)	0	0	33.8(4)	63.1(2)	45.3(1)	0	44.1(1)

[a] A, B, C, and D define the pyrrole rings containing N1, N2, N3, and N4. [b] The roof folding is defined as the angle between the planes containing the two halves of the ligand (first half: pyrrole A, *meso* sp^2 carbon C5, pyrrole B; second half: pyrrole C, *meso* sp^2 carbon C15, pyrrole D).

Table 3. Selected bond lengths [Å] for compounds **4**–**6** and **8**–**14**.

	5	**8**	**9**	**10**	**11**	**14**	**6**	**4**	**12**	**13**
M–N_{av}	1.935(3)	2.130(2)	1.937(2)	2.124(3)	2.128(2)	2.004(5)	1.893(3)	1.952(2)	2.098(2)	1.980(1)
M–L_{ax} (av)	–	2.187(2)	2.169(2)	2.353(3)	2.420(2)	2.373(2)	–	–	2.248(1)	1.989(1)

differences stem in general from two important structural features: coordination of the metal ion and conformation of the ligand.

The coordination is in both cases square-pyramidal. It is almost perfect in the case of compound **9**, in which the Co^{II} is only displaced by −0.0519(10) Å from the N_4 plane. In compound **8** the geometry is distorted and the deviation of the Mn^{II} ion from the N_4 plane is −0.298(1) Å. The average M–N distance is 1.938(2) Å in **9** and 2.130(2) Å in **8**, reflecting also the different spin states and the radii of the two metal ions [HS-Mn^{II}, 0.82 Å; LS-Co^{II}, 0.65 Å].

The ligand shows a large roof folding angle, with a high degree of ruffling (see Table 2) in compound **9**, while it is in a quasi-planar arrangement, with a little folding, in compound **8**.

The flexibility of the ligand also influences the disposition of the axial ligand in both complexes. In compound **9**, in which no strong steric effect between the ethyl chains and the pyridine is present, the ligand is oriented along the axis that links the *meso* sp^3 carbon atoms [N2-Co1-N5-C33 = 45.0(2)°; N3-Co1-N5-C33 = −45.2(2)°], whereas in complex **8** the steric hindrance orients the THF molecule along the C5···C15 axis [N1-Mn1-O1-C36 = −49.8(2)°, N2-Mn1-O1-C36 = 40.2(2)°]. Intermolecular interactions occur only in compound **9** between the Co^{II} and hydrogen atoms belonging to ethyl chains (Co1···H29B = 2.83 Å, Co1 − H23B = 3.18 Å).

© WILEY-VCH Verlag GmbH, D-69451 Weinheim, 2001
0947-6539/01/0712-2538 $ 17.50+.50/0 *Chem. Eur. J.* **2001**, *7*, No. 12

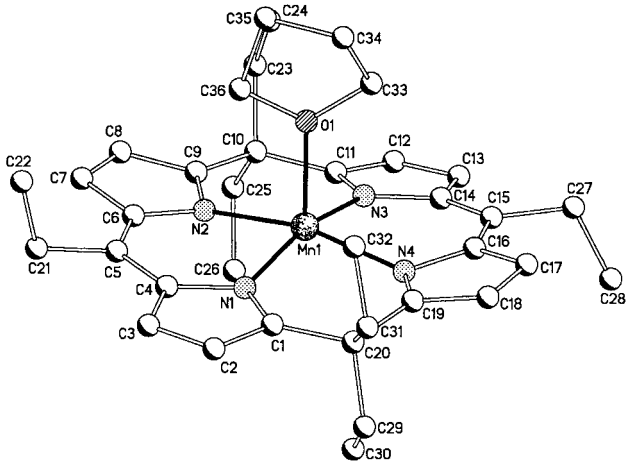

Figure 2. XP drawing of **8** with the labeling scheme adopted (H atoms omitted for clarity).

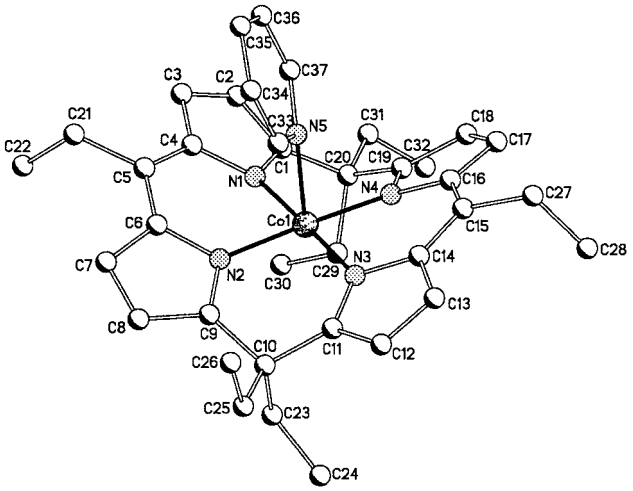

Figure 3. XP drawing of **9** with the labeling scheme adopted (H atoms omitted for clarity).

*Complexes **10** and **11***: These two compounds are very similar, and they are depicted in Figures 4 and 5, respectively. They both exhibit slightly distorted octahedral geometry of the metal ion [Mn^{II}], without any out-of-plane deviation (for symmetry requirements) from the N_4 core. The average $Mn-N_{core}$ bond length is 2.124(3) Å for **10** and 2.128(2) Å[5] for **11**. The equatorial ligands are in both cases almost planar (see Table 2) with a small ruffling. The mean planes of the axial ligands are, roughly speaking, oriented along the axis linking the two *meso* sp^2 carbon atoms. This is due to the steric hindrance between the methyl hydrogen atoms and the hydrogen atoms belonging to the ligands (THF for **10**, pyridine for **11**). Such dispositions are attested by the following torsion angles: N1-Mn1-O1-C17 = −38.3(3)°, N2-Mn1-O1-C17 = 52.2(3)° for **10**; N1-Mn1-N3-C21 = 60.6(2)°, N2-Mn1-N3-C21 = −29.4(2)° for **11**. No particular inter- or intramolecular interaction has been observed in the solid state for either structures.

*Complex **14***: In complex **14** (Figure 6) the metal center is surrounded by five atoms in a distorted square-pyramidal arrangement and is displaced from the N_4 plane by

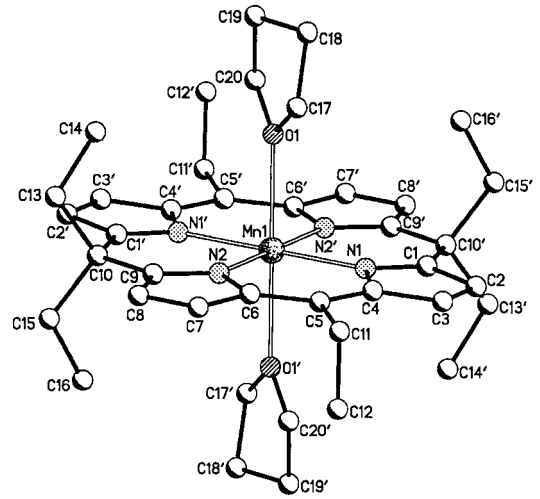

Figure 4. XP drawing of **10** with the labeling scheme adopted (H atoms omitted for clarity). A prime denotes the following symmetry transformation: $-x, -y, -z$.

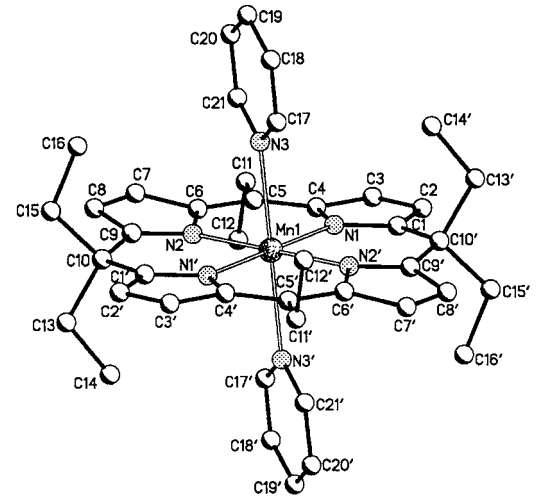

Figure 5. XP drawing of **11** with the labeling scheme adopted (H atoms omitted for clarity). A prime denotes the following symmetry transformation: $-x, -y, -z$.

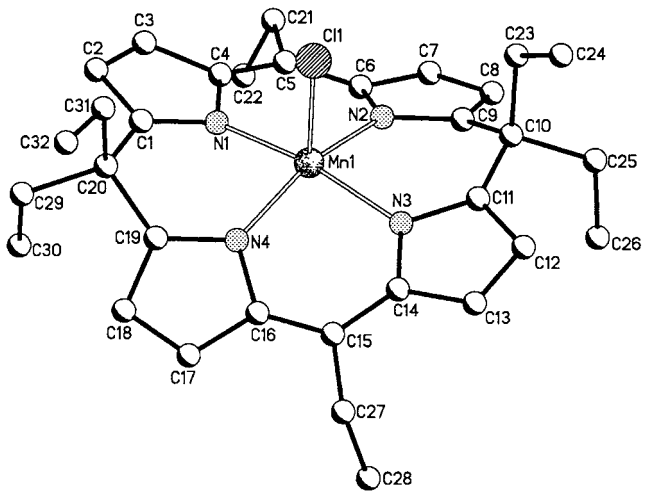

Figure 6. XP drawing of **14** with the labeling scheme adopted (H atoms omitted for clarity).

– 0.303(3) Å. The Mn–N bond lengths vary in a narrow range [1.993(5) – 2.013(5) Å] and the Mn–Cl bond length is 2.373(2) Å. The ligand shows the usual roof conformation (see Table 2) with a significant ruffling giving the saddle form. The distance between the two *meso* sp^2 carbon atoms is, as expected, shorter than that calculated for the two sp^3 carbon atoms [C5 ··· C15 = 6.711(9) Å versus C10 ··· C20 = 6.945(9) Å]. The solid-state structure shows some interactions between the metal and one methyl hydrogen of an ethyl chain in a neighboring molecule (Mn ··· H = 2.77 Å), thus spawning a pseudo-octahedral geometry. Also noteworthy are some intramolecular hydrogen bonds involving the chlorine atom (Cl1 ··· H23B = 2.70 Å and Cl1 ··· H31A = 2.72 Å).

Structural and spectroscopic properties: **Optical spectra**: All the metal porphodimethene complexes were characterized by UV/Vis spectroscopy. The optical spectra in benzene of the unsolvated complexes are reported in Figure 7 and are all

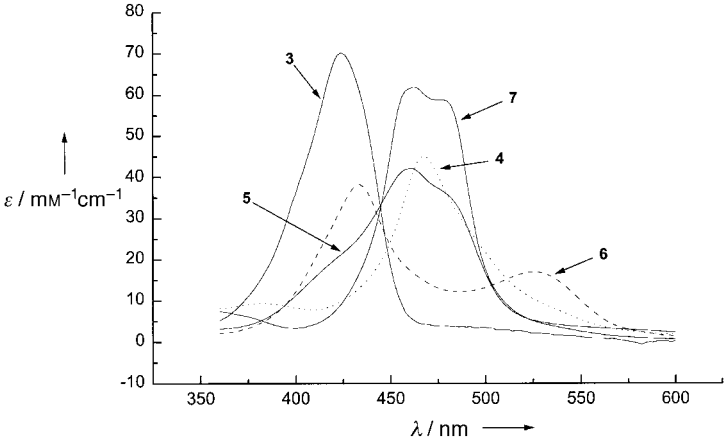

Figure 7. The UV/Vis spectra of the unsolvated complexes **3** – **7**.

characterized by the presence of an intense absorption maximum between 420 and 470 nm with a shoulder at 480 – 490 nm for Co and Cu, or a second weaker band at around 500 nm for Fe and 530 nm for Ni. These absorption bands are similar to those observed for other metallodiporphomethenes[3b, 3h, 6] and originate from π to π* ligand transitions,[6c] see below. The electronic absorption spectra of these metal porphodimethenes bear some resemblance to those of the corresponding metal porphyrins, which are characterized by an intense transition at 400 – 420 nm (the Soret or B band) and a pair of vibrationally resolved weak transitions at 550 – 600 nm (the Q bands) and which have been assigned to single excitations from a_{1u}, a_{2u} porphyrin π to e_g* porphyrin π* orbitals, forming four excited states which can mix by configuration interaction.[7] In the metal porphodimethenes, however, the Soret band is replaced by a characteristic "methene" band at lower energy (420 – 470 nm) with a smaller extinction coefficient. At variance with this band, the energy and the intensity of the second weaker peak at higher energy depends on the nature of the metal and is also strongly affected by the presence of axial ligands, as exemplified by the optical spectra of the solvated complexes of manganese with one THF, two THF or two pyridine molecules, see Figure 8.

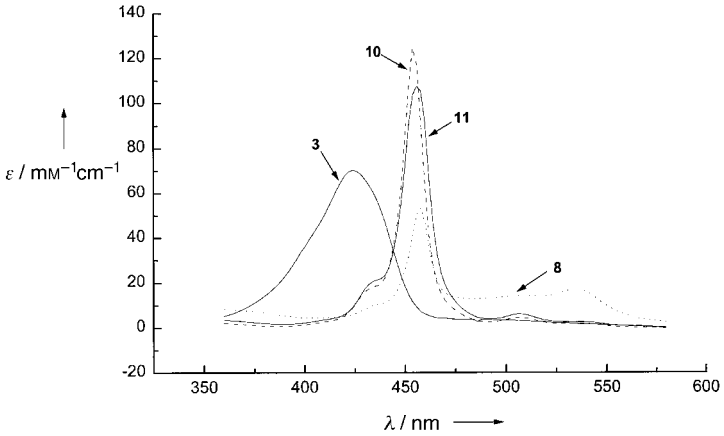

Figure 8. The UV/Vis spectra of the solvated complexes **3**, **8**, **10**, and **11**.

Magnetic properties: The magnetic susceptibilities of complexes **3** – **14** were measured in the temperature range 1.9 – 300 K. Those of **3** – **5** and **9** are shown in Figures 9 – 12.

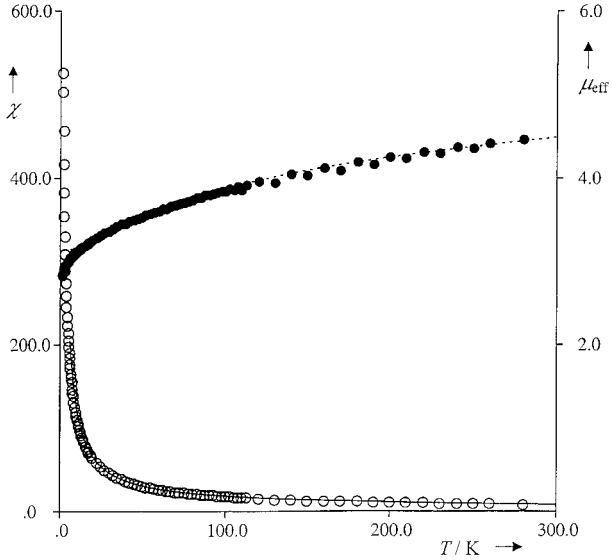

Figure 9. Magnetic susceptibilities (○), 10^{-3} emu, and magnetic moments (●), μ_B, as a function of the temperature for complex **3**.

The magnetic moment of the four-coordinate manganese complex **3** has a value of 4.0 μ_B at 298 K, which remains almost constant between 300 and 100 K and then decreases suddenly, reaching a value of 3.0 μ_B at 2.0 K (see Figure 9). This behavior is compatible with a $S = 3/2$ intermediate spin state, with a magnetic moment at room temperature slightly larger than the spin-only value of 3.88 μ_B. It is worth noting that the analogous tetracoordinated manganese(II) phthalocyanine has a $S = 3/2$ ground state with a large value of the magnetic moment at room temperature (ca. 4.4 μ_B).[8]

The magnetic data have been analyzed in terms of an isolated $S = 3/2$ state with an isotropic g factor and an axial zero-field splitting described by the spin Hamiltonian in Equation (1),[9] where $S = 3/2$ and D is the zero-field splitting

$$\mathscr{H} = \beta g \mathscr{H} \cdot \boldsymbol{S} + D[\boldsymbol{S}_z^2 - S(S+1)/3] \quad (1)$$

© WILEY-VCH Verlag GmbH, D-69451 Weinheim, 2001
0947-6539/01/0712-2540 $ 17.50+.50/0 *Chem. Eur. J.* **2001**, *7*, No. 12

constant. The spin degeneracy of the $S = 3/2$ state is partly lifted by spin–orbit coupling into the $M_s = \pm 1/2$ and $M_s = \pm 3/2$ components, separated by the zero-field splitting parameter $2D$. The magnetic susceptibility can be derived by the Van Vleck Equation and is given by Equation (2),[9] with

$$\chi_{dim} = \frac{Ng^2\mu_B^2}{kT} \frac{{}^3/_4(1 + \exp(-2x)) + \left(\frac{1}{2}x\right)(1 - \exp(-2x))}{1 + \exp(-2x)} \quad (2)$$

$x = D/kT$. A temperature-independent paramagnetism (TIP) term N_α was also included to account for the slight increase of the magnetic moment with T, which is still observed close to room temperatures. A good fit was found for $g = 2.05$, $D = 98\,cm^{-1}$, and $N_\alpha = 1.8 \times 10^{-4}$ (see the solid line in Figure 9). The relatively high TIP value is due to the presence of a low-lying high-spin state, as confirmed by the DFT calculations (see below).

A different behavior is observed for the THF-coordinated manganese complexes **8** and **10**, whose magnetic moments are constant throughout most the temperature range 2–300 K, with a value of about 5.9 μ_B clearly indicating a high-spin ($S = 5/2$) Mn^{II} d^5 species.

The temperature dependence of the magnetic moments of the iron complex **4** is illustrated in Figure 10. The magnetic moment is almost constant between 50 and 300 K with a

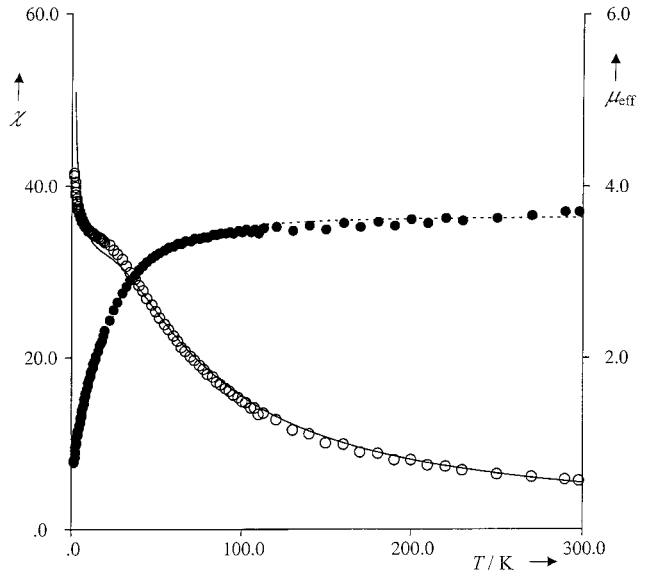

Figure 10. Magnetic susceptibilities (○), 10^{-3} emu, and magnetic moments (●), μ_B, as a function of the temperature for complex **4**.

room-temperature value of 3.45 μ_B at 300 K, and shows a sudden decrease below 50 K, dropping to 0.95 μ_B at 2 K. The room-temperature value of the effective magnetic moment is consistent with an $S = 1$ intermediate-spin state, while the decrease at low temperature can be attributed to a large zero-field splitting with a nonmagnetic level lying lowest. This behavior is quite similar to that of other tetracoordinated Fe^{II} complexes with square-planar coordination constituted by an N_4 macrocyclic ligand.[10, 11] The room-temperature value for **4** is very close to that reported for Fe(Pc) (Pc = phthalocyanine), $\mu_{eff} = 3.9\ \mu_B$,[10] and slightly lower than that of Fe(TPP) (TPP = tetraphenylporphyrin), $\mu_{eff} = 4.2\ \mu_B$.[11] These data have already been analyzed in terms of an isolated $S = 1$ spin state using the spin Hamiltonian [Eq. (1)], and a good fit was found for $g = 2.49$, $D = 71.5\ cm^{-1}$;[12] see solid line in Figure 10.

The temperature dependence of the magnetic moments of the cobalt pyridine complex **9** indicates a monomeric low-spin Co^{II} d^7 species, the magnetic moment being nearly constant over the whole temperature range with a value of ca. 2.20 μ_B (Figure 11). Although much larger than the spin-only values of 1.73, the magnetic moment of **9** is close to the values observed for other Co^{II} ions in square-planar and square-pyramidal coordination.[13]

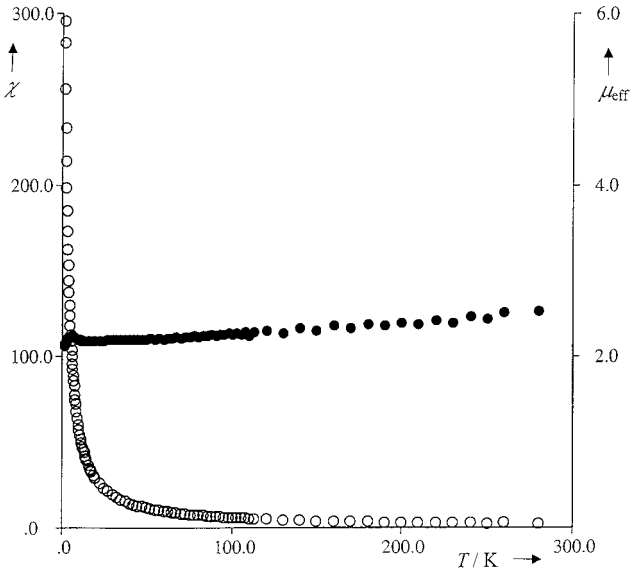

Figure 11. Magnetic susceptibilities (○), 10^{-3} emu, and magnetic moments (●), μ_B, as a function of the temperature for complex **9**.

Similar behavior is observed for the unsolvated cobalt complex **5**, which, however, has a higher value for the room-temperature magnetic moment (approx. 2.50 μ_B) and a slight increase of the magnetic moment below 20 K (Figure 12), probably due to weak intermolecular magnetic coupling between the metal centers within the crystal structure. It is worth noting that analogous intermolecular ferromagnetic interactions have been observed for some planar macrocyclic complexes such as manganese(II) phthalocyanine, which has a stacked crystal structure in which two azomethine nitrogen atoms of each molecule lie above or below the metal atom belonging to nearest neighbors.[14]

The nickel complex **6** is diamagnetic, indicating a low-spin $S = 0$ state, as expected for a Ni^{II} d^8 metal center in square-planar coordination.

The magnetic moments of the copper complex **7** demonstrate the typical behavior of Cu^{II} d^9 species, being nearly constant over the whole temperature range, with a value of ca. 1.73 μ_B.

Theoretical studies: density functional investigations: We performed density functional calculations in order to gain a deeper insight into the geometric and electronic structure of

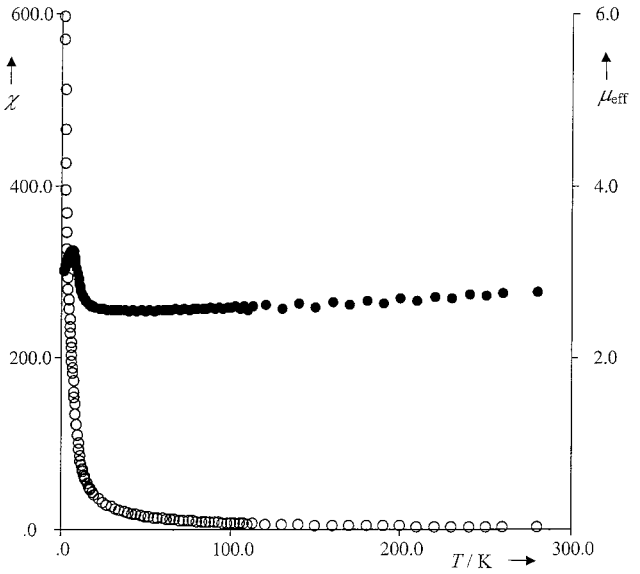

Figure 12. Magnetic susceptibilities (○), 10^{-3} emu, and magnetic moments (●), μ_B, as a function of the temperature for complex **5**.

these porphodimethene metal complexes. DFT calculations including nonlocal correction to the exchange-correlation potential have been recently shown to describe adequately the geometry and the energy ordering of the lowest spin states of metalloporphyrins.[15]

Since the iron porphodimethene complexes have already been studied in a previous work,[12] we will address here only Mn, Co, Ni, and Cu complexes. Several possible spin states have been considered for each metal, namely $S = ½, 3/2, 5/2$ for Mn^{II}; $S = ½, 3/2$ or Co^{II}; and $S = 0, 1$ for Ni^{II}. The ground states depend on the relative energies of the metal d orbitals, which in turn depend on the ligand field of the porphodimethene macrocycle and of any axial ligands. The main structural parameters, including macrocycle conformation and deviation of the metal from the N_4 plane, are determined by these fields. Geometry optimizations in C_{2v} symmetry have been performed for the lowest spin states of all considered complexes. The essential results of these calculations are reported in Table 4, which shows the relative energies and the metal configurations of the lowest spin states for each metal complex. Table 4 shows that the ground state is a $^4A_2$ intermediate-spin state for Mn and a low-spin state for Co and Ni ($^2A_1$ and $^1A_1$, respectively), in agreement with the magnetic data. Density functional calculations at the same level of accuracy have been recently performed on iron(II) porphodimethenes[12] and have shown that the ground state is a $^3B_1$ intermediate-spin state.[12]

Density functional calculations have also been performed for the manganese complex with an axial water molecule in order to simulate the THF complex **8**. The results (see Table 4) show, at variance with the uncoordinated molecule, a high-spin $^6A_1$ ground state in agreement with the magnetic evidence.

Table 5 reports the optimized geometries for the ground states of the considered porphodimethene metal complexes. As in the X-ray structures, the calculated geometries are not planar but display a rooflike folding along the line joining the two saturated *meso*-carbon atoms and a ruffling distortion along each dipyrromethene half. The folding is specified by

Table 4. Energies calculated for the lowest lying electronic states of the metal porphodimethenes under consideration.

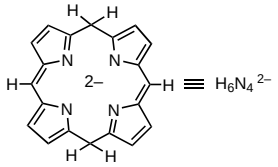

System	State	Configuration	ΔE [eV]
$[(H_6N_4)Mn]$	$^4A_2$	$(d_{x^2-y^2})^2(d_{yz})^1(d_{xy})^1(d_{z^2})^1$	0.00
	$^6A_1$	$(d_{x^2-y^2})^1(d_{z^2})^1(d_{xz})^1(d_{yz})^1(d_{xy})^1$	0.15
	$^2A_1$	$(d_{x^2-y^2})^2(d_{xz})^2(d_{yz})^2(d_{z^2})^1$	0.53
$[(H_6N_4)Mn(H_2O)]$	$^6A_1$	$(_{x^2-y^2})^1(d_{z^2})^1(d_{xz})^1(d_{yz})^1(d_{z^2})^1$	0.00
	$^4A_2$	$(d_{x^2-y^2})^2(d_{xz})^1(d_{yz})^1(d_{z^2})^1$	0.10
$[(H_6N_4)Co]$	$^2A_1$	$(d_{x^2-y^2})^2(d_{xz})^2(d_{yz})^2(d_{z^2})^1$	0.00
	$^4B_1$	$(d_{x^2-y^2})^2(d_{xz})^2(d_{yz})^1(d_{z^2})^1(d_{xy})^1$	0.74
$[(H_6N_4)Ni]$	$^1A_1$	$(d_{x^2-y^2})^2(d_{xz})^2(d_{yz})^2(d_{z^2})^2$	0.00
	$^3B_2$	$(d_{x^2-y^2})^2(d_{xz})^2(d_{yz})^2(d_{z^2})^1(d_{xy})^1$	0.83

Table 5. Pertinent geometrical parameters obtained for the ground states of the Mn, Fe, Co, and Ni porphodimethene complexes.

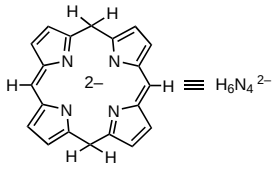

System			M–N	N–C_1	N–C_4	C_1–C_2	C_2–C_3	C_3–C_4	C_4–C_5	OOP	α	β
$[(H_6N_4)Mn]$	($S = 3/2$)	calcd	2.036	1.360	1.408	1.415	1.386	1.422	1.388	0.08	30.5	9.2
$[(H_6N_4)Mn]$	($S = 5/2$)	calcd	2.131	1.345	1.394	1.421	1.384	1.425	1.395	0.03	19.1	5.4
$[(Et_6N_4)Co]$ (**5**)		X-ray	1.935	1.35	1.41	1.42	1.36	1.42	1.39	0.02	44.4	25.6
$[(H_6N_4)Co]$	($S = ½$)	calcd	1.989	1.351	1.402	1.422	1.383	1.425	1.387	0.07	41.4	13.3
$[(Et_6N_4)Ni]$ (**6**)		X-ray	1.893	1.337	1.408	1.423	1.383	1.420	1.387	0.07	63.1	20.4
$[(H_6N_4)Ni]$	($S = 0$)	calcd	1.975	1.351	1.402	1.422	1.383	1.425	1.387	0.07	40.1	13.7
$[(Et_6N_4)Cu]$ (**7**)		X-ray	1.979	1.353	1.388	1.414	1.356	1.433	1.393	0.04	40.3	19.5
$[(H_6N_4)Cu]$	($S = ½$)	calcd	2.034	1.345	1.396	1.425	1.385	1.428	1.393	0.06	40.3	10.7
$[(Et_6N_4)Mn(THF)]$ (**8**)		X-ray	2.130	1.345	1.416	1.423	1.361	1.423	1.404	−0.30	11.2	10.5
$[(H_6N_4)Mn(H_2O)]$	($S = 5/2$)	calcd	2.145	1.345	1.396	1.426	1.385	1.429	1.399	0.30	32.7	6.9

© WILEY-VCH Verlag GmbH, D-69451 Weinheim, 2001
0947-6539/01/0712-2542 $ 17.50+.50/0 *Chem. Eur. J.* **2001**, *7*, No. 12

the angle between the normals to the planes defined by the two dipyrromethene halves (ϕ), while the ruffling is specified by the angles between the normals to adjacent pyrrole ring within each dipyrromethene half (θ) and can therefore be directly compared with the X-ray results, in other words, respectively, the last line and the average of angles between AB and CD in Table 2. In Table 2 we also report the deviation of the metal from the N_4 mean plane, and the pertinent bond lengths, based on the numbering scheme used in Scheme 1.

Table 5 shows that the calculated geometries of the metalloporphodimethenes are in fairly good agreement with crystallographic data. In particular the computed bond length scheme is in accordance with the simple resonance description of the π-electron delocalization within each dipyrromethene half illustrated in Scheme 3. The only significant deviations concern the M–N core sizes for the unsolvated complexes, for which the calculated lengths overestimate the experimental values by ca. 0.05 Å. However, this discrepancy could be due to the presence of ethyl groups at the *meso* carbons in the actual complexes and packing constraints in the crystals that may enhance the rooflike and ruffling distortions, thus leading to shorter M–N core lengths. Indeed, an analysis of metal porphyrin complexes[16] demonstrated that a ruffling of the core could allow a shortening of the M–N bonds while not necessarily requiring substantial alterations in other distances within the ligand. This is supported by the fact that for the planar pentacoordinated manganese complex **8**, where no ruffling is observed, there is an excellent agreement between the calculated and experimental Mn–N bond distance, 2.145 vs. 2.130 Å.

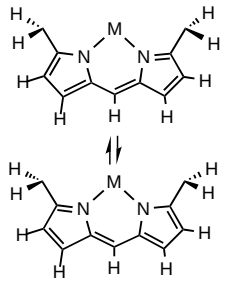

Scheme 3. Resonance description of each dipyrromethene half.

It is worth noting that there is a rather good agreement between the Mn–N and the other intraligand bond lengths calculated for the high-spin state of the unsolvated manganese complex and the crystallographic data for the corresponding high-spin pentacoordinate manganese(II) complexes **8**, suggesting that the axial ligands have little effect on the metal porphodimethene geometry.

Table 5 also shows that the length of the M–N core is determined mainly by the electronic state and specifically by the occupancy of the antibonding d_{xy} orbital. In particular the core size for the manganese high-spin state (with occupied d_{xy}) is significantly larger than for the manganese intermediate-spin state or for the cobalt and nickel low-spin states; a relatively large core size is also observed for the copper complex whose doublet ground state shows an occupied d_{xy} orbital. This behavior is quite similar to that observed for the corresponding metal porphyrin complexes.[17]

Slight but significant differences between the M–N core sizes of porphyrin and porphodimethene metal complexes need to be mentioned. The core size of tetracoordinated metal porphodimethenes is invariably less than that of the corresponding porphyrin complexes: 1.952 Å for **4** vs. 1.972 Å for [Fe(TTP)][18] or 1.996 Å for [Fe(OEP)];[19] 1.935 Å for **5** vs. 1.950 Å for [Co(TTP)][20] or 1.979 Å for [Co(OEP)];[21] 1.890 Å for **6** vs. 1.928 Å for [Ni(TTP)][22] or 1.952 Å for [Ni(OEP)];[23] 1.979 Å for **7** vs. 1.981 Å for [Cu(TTP)][24] or 1.998 Å for [Cu(OEP)].[25] This is because of the flexibility of the porphodimethene ligand, which may fold and achieve a higher degree of ruffling than the porphyrins, thus allowing a shortening of the M–N bonds. However, when planar unruffled complexes are considered, the M–N core size of porphodimethenes may be larger than those of the corresponding porphyrins, as illustrated by the Mn–N bond length in **8**, 2.130 Å, which is slightly larger than that in [Mn(TTP)(1-MeIm)], 2.128.[5] This is probably due to the intrinsically larger macrocycle coordination cavity of the porphodimethene ligand, as a consequence of the two *meso* sp^3 carbons, with the longer σ(C–C) bonds connecting them to the adjacent pyrrole rings.

It is interesting to compare the electronic structure of these metal porphodimethene complexes with those of the corresponding porphyrin systems, which have been the subject of several experimental and theoretical studies.[26]

Four-coordinate Mn^{II} porphyrins are all high-spin species with a $^6A_1\ (d_{x^2-y^2})^1(d_{z^2})^1(d_{xz})^1(d_{yz})^1(d_{xy})^1$ ground state. A different $^4A_2\ (d_{x^2-y^2})^2(d_{z^2})^1(d_{xz})^1(d_{yz})^1$ intermediate-spin ground state is found for the Mn^{II} porphodimethene complex, as suggested by the magnetic data and confirmed by the theoretical calculations. This difference is not easy to explain, since the larger macrocycle coordination cavity of the porphodimethene ligand (as a consequence of the two *meso* sp^3 carbons) is expected to stabilize the d_{xy} orbital and thus the high-spin state. However, the porphodimethene macrocycle is also more flexible than its porphyrin counterpart and can better adapt the smaller intermediate-spin Mn^{II} radius through combined rooflike and ruffling deformations, thus actually behaving as if it has a smaller coordination cavity. This is illustrated by the X-ray structure of the rooflike deformed and ruffled Fe^{II} porphodimethene **4**, which has a smaller Fe–N core size, (1.972 Å),[13] than that of the planar Fe^{II} porphyrin complex [Fe(OEP)] (1.996 Å).[14] It is worth noting that an intermediate-spin state has been observed for Mn^{II} phthalocyanine derivatives,[8] the phthalocyanine macrocycle having a smaller coordination cavity than porphyrins.

On the other hand, Fe^{II}, Co^{II}, and Ni^{II} porphodimethenes show the same spin states observed for the corresponding metal porphyrins, namely, an intermediate-spin state for Fe^{II} and low-spin states for Co^{II} and Ni^{II}.[17]

In an attempt to investigate the reasons for this difference and to compare the electronic structure of the metal porphodimethene and porphyrin complexes, we performed DFT calculations, at the same level of theory, on the $^1A_1$ ground state of nickel(II) porphyrin under D_{4h} symmetry constraints. In Figure 13, we compare the main frontier orbitals for the two complexes obtained from spin-restricted DFT calculations performed on the optimized geometries of the same $^1A_1$ state. The metal orbitals for the two complexes are quite similar, the pertinent differences being: (1) a higher energy of the metal orbitals (especially the d_{xy}) in the porphodimethene complex, and (2) the energy splitting in the porphodimethene complex of the degenerate $e_g(d_{xz}, d_{yz})$

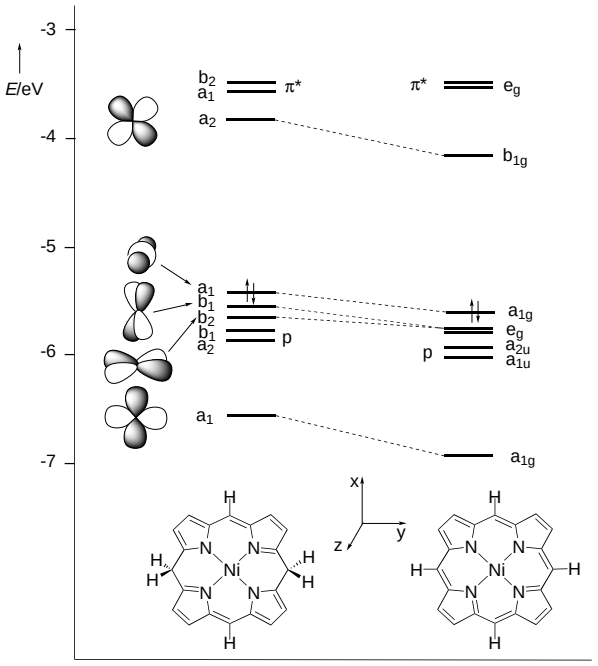

Figure 13. Molecular orbital diagram for nickel(II) porphodimethene and porphyrin complexes.

level of the iron porphyrin with a slight stabilization of the $b_1(d_{xz})$ lying in the plane containing the two saturated *meso* carbon atoms. In particular the significant energy increase of the d_{xy} orbital is associated with the smaller M–N core size achieved in the porphodimethene (1.960 vs. 1.980 Å) and is expected to destabilize high-spin states and is probably responsible for the observed intermediate-spin ground state observed for the tetracoordinated manganese(II) complex **3**.

A second important difference is the energy splitting of the lowest unoccupied $e_g(\pi^*)$ orbital of the metal porphyrin into the b_2 and a_1 in the porphodimethene and the higher energy of the two highest porphodimethene π orbitals a_2 and b_1 with respect to the porphyrin. Since these two orbitals are involved in the intense $\pi \rightarrow \pi^*$ transition that gives rise to the two main bands in the electronic absorption spectra of these complexes, these orbital changes are responsible for the observed differences between metal porphodimethene and porphyrin absorption spectra. In particular the energy increase of π orbitals is expected to lead to a red shift of the main methene band with respect to the Soret band.

Experimental Section

General procedure: All reactions were carried out under an atmosphere of purified nitrogen. Solvents were dried and distilled before use by standard methods. Infrared spectra were recorded with a Perkin–Elmer FT 1600 spectrophotometer; UV/Vis spectra were recorded with a Hewlett-Packard 8452A diode array spectrophotometer.

Magnetic susceptibility was measured with an MPMS5 SQUID susceptometer (Quantum Design) operating at a magnetic field strength of 1 kOe. Corrections were applied for diamagnetism calculated from Pascal constants.[27] Effective magnetic moments were calculated as $\mu_{eff} = 2.828(\chi_{Fe} \cdot T)^{1/2}$, where χ_{Fe} is the magnetic susceptibility per iron center. The magnetic data were fitted to the theoretical expression by minimization of the agreement factor, defined as $\Sigma\frac{[\chi_i^{obsd}T_i - \chi_i^{calcd}T_i]^2}{\chi_i^{obsd}T_i}$, by means of a Levenberg–Marquardt routine.

Computational and methodological details. The calculations reported in this paper are based on the ADF (Amsterdam Density Functional) program package described elsewhere.[28] Its important characteristics are the use of a density fitting procedure to obtain accurate Coulomb and exchange potentials in each SCF cycle, the accurate and efficient numerical integration of the effective one-electron Hamiltonian matrix elements, and the possibility of freezing core orbitals. The molecular orbitals were expanded in an uncontracted double-zeta STO basis set for all atoms, with the exception of the transition metal orbitals, for which we used a double-zeta STO basis set for 3s and 3p and a triple-zeta STO basis set for 3d and 4s. As polarization functions one 4p, one 3d, and one 2p STO were used for transition metals, O and C, and H, respectively. The cores (Mn, Fe, Co, Ni: 1s–2p; C, O, N: 1s) were kept frozen. The LDA exchange correlation potential and energy were used, together with the Vosko–Wilk–Nusair parametrization[29] for homogeneous electron gas correlation, including Becke's nonlocal correction[30] to the local exchange expression and Perdew's nonlocal correction[31] to the local expression of correlation energy (NLDA). It has been demonstrated that excellent metal–metal and ligand–metal bond energies are obtained from this DFT approach.[32]

Molecular structures were optimized by the NLDA method, thanks to the successful implementation of analytical energy gradients in C_{2v} (or C_2) symmetry. The way in which the nonlocal corrections improve optimized geometries of transition metal complexes has already been demonstrated, especially for metal–ligand bond lengths, otherwise almost uniformly too short (by about 0.05 Å) when calculated by local methods.[32]

The syntheses of **1**,[4] **2**,[4] **4**,[16] **6**,[4] **12**,[12] **13**,[12] and $[Mn_3Mes_6]$[33] [Mes ≡ 2,4,6-$Me_3C_6H_2$] have been carried out as reported in the literature.

Synthesis of [(Et_6N_4)Mn] (3): $[Mn(Mes)_2]_3 \cdot$ tol (1.34 g, 1.39 mmol) was added to a solution of **2** (2.00 g, 4.16 mmol) in benzene (100 mL). The amber solution obtained was stirred overnight at room temperature. The solvent was evaporated and the residue triturated with *n*-pentane (100 mL) to give a dark orange powder which was collected and dried in vacuo (1.33 g, 60%). UV/Vis (C_6H_6): λ_{max} (ε) = 424 nm (66100 $mol^{-1} dm^3 cm^{-1}$); elemental analysis calcd (%) for **3**, $C_{32}H_{38}MnN_4$ (533.6): C 72.03, H 7.18, N 10.50; found C 72.25, H 7.19, N 10.23.

Synthesis of [(Et_6N_4)Co] (5): $CoCl_2(THF)_{1.5}$ (9.12 g, 38.32 mmol) was added to a solution of **1** (21.86 g, 38.50 mmol) in benzene (500 mL). The solution was stirred overnight at room temperature and then refluxed for two hours. Lithium chloride was filtered off and the solvent was evaporated to dryness. *n*-Hexane (150 mL) was added to give a brown powder, which was collected and dried in vacuo (14.0 g, 72%). Crystals suitable for X-ray analysis were obtained in benzene/*n*-hexane. UV/Vis (C_6H_6): λ_{max} (ε) = 460 (39900), 478 sh nm (34800 $mol^{-1} dm^3 cm^{-1}$); elemental analysis calcd (%) for **5**, $C_{32}H_{38}CoN_4$ (537.6): C 71.49, H 7.12, N 10.42; found C 71.59, H 7.11, N 10.62.

Synthesis of [(Et_6N_4)Cu] (7): $CuCl_2(THF)_{0.5}$ (1.01 g, 5.94 mmol) was added to a solution of **1** (3.61 g, 5.94 mmol) in benzene (200 mL). The reaction mixture became dark with a yellow reflection. The mixture was stirred overnight at room temperature and then refluxed for 2 h. LiCl was filtered off and the solvent was evaporated to dryness. *n*-Pentane (80 mL) was added to give a microcrystalline product (1.75 g, 54%). Recrystallization from benzene/pentane gave crystals which were suitable for X-ray analysis. UV/Vis (C_6H_6): λ_{max} (ε) = 464 (62000), 480 sh nm (58800 $mol^{-1} dm^3 cm^{-1}$); elemental analysis calcd (%) for **7**, $C_{32}H_{38}CuN_4$ (542.2): C 70.88, H 7.06, N 10.33; found C 70.42, H 7.01, N 10.22.

Synthesis of [(Et_6N_4)Mn(THF)] (8): $MnCl_2(THF)_{1.5}$ (1.92 g, 8.2 mmol) was added to a solution of **1** (5.22 g, 8.2 mmol) in benzene (200 mL). The solution was stirred overnight at room temperature and then refluxed for 2 h. LiCl was filtered off and the resulting orange solution was evaporated to dryness; *n*-hexane (70 mL) was added to give a purple powder, which was collected and dried in vacuo (3.62 g, 73%). Crystals suitable for X-ray analysis were obtained in benzene/*n*-hexane. IR (nujol): $\tilde{\nu}_{max}$ = 1560.2 (s), 1511.1 (m), 1494.4 (m), 1455.6 (m), 1374.8 (m), 1334.4 (m), 1301.9 (s), 1277.8 (m), 1239.7 (s), 1189.9 (w), 1105.6 (w), 1062.9 (s), 996.7 (s), 888.3 (w), 843.7 (m), 772.8 (m), 727.7 (m) cm^{-1}. UV/Vis (C_6H_6): λ_{max} (ε) = 458 (53500), 534 nm (15200 $mol^{-1} dm^3 cm^{-1}$); elemental analysis calcd (%) for **8**, $C_{36}H_{46}MnN_4O$ (605.7): C 71.38, H 7.65, N 9.25; found: C 71.13, H 7.69, N 9.62.

© WILEY-VCH Verlag GmbH, D-69451 Weinheim, 2001
0947-6539/01/0712-2544 $ 17.50+.50/0 *Chem. Eur. J.* **2001**, *7*, No. 12

Synthesis of [(Et_6N_4)Co(Py)] (9): Pyridine (2 mL) was added to a solution of **5** (1.91 g, 3.56 mmol) in THF (100 mL). The solvent was evaporated to dryness. *n*-Hexane (50 mL) was added to give a blue-violet crystalline product which was collected and dried in vacuo (1.8 g, 82 %). Crystals suitable for X-ray diffraction were grown in a mixture of THF/*n*-hexane. UV/Vis (C_5H_5N): λ_{max} (ε) = 452 nm (99 400 $mol^{-1} dm^3 cm^{-1}$); elemental analysis calcd (%) for **9**, $C_{37}H_{43}CoN_5$ (616.7): C 72.06, H 7.03, N 11.35; found C 72.21, H 7.15, N 11.43.

Synthesis of [(Et_6N_4)Mn(THF)$_2$] (10): A solution of **8** (2.21 g, 3.65 mmol) in THF (20 mL) was stirred for 2 h at room temperature. *n*-Pentane (60 mL) was added dropwise and the product was collected and dried in vacuo (0.51 g, 20 %). Crystals suitable for X-ray analysis were obtained in benzene/*n*-hexane. IR (nujol): $\tilde{\nu}_{max}$ = 1560.7 (s), 1505.6 (w), 1488.9 (w), 1458.4 (m), 1375.6 (m), 1327.8 (w), 1294.0 (s), 1240.3 (s), 1065.8 (s), 1004.4 (s), 844.5 (m), 777.8 (m), 750.0 (m), 725.5 (m) cm^{-1}; UV/Vis (THF): λ_{max} (ε) = 430 sh (19 900), 454 (12 4400), 506 nm (5800 $mol^{-1} dm^3 cm^{-1}$); elemental analysis calcd (%) for **10**, $C_{40}H_{54}MnN_4O_2$ (677.8): C 70.88, H 8.03, N 8.27; found C 70.81, H 7.95, N 8.09.

Synthesis of [(Et_6N_4)Mn(Py)$_2$] (11): A solution of **8** (1.14 g, 1.88 mmol) in benzene (100 mL) was treated with an excess of pyridine (0.45 g, 5.69 mmol). The solution was stirred overnight at room temperature. The solvent was evaporated to dryness and *n*-hexane (50 mL) was added to give a purple powder that was collected and dried in vacuo (0.63 g, 70 %). Recrystallization of the powder from THF/*n*-hexane gave crystals suitable for X-ray analysis. IR (nujol): $\tilde{\nu}_{max}$ = 1562.2 (s), 1511.1 (m), 1494.4 (m), 1455.0 (m), 1373.9 (m), 1334.0 (m), 1305.6 (s), 1277.7 (m), 1236.3 (s), 1183.3 (w), 1138.9 (w), 1105.6 (w), 1065.1 (s), 1038.9 (w), 998.7 (s), 840.7 (m), 770.5 (m), 715.4 (m) cm^{-1}; UV/Vis (C_5H_5N): λ_{max} (ε) = 432 sh (31 900), 456 (10 7600), 506 nm (7900 $mol^{-1} dm^3 cm^{-1}$); elemental analysis calcd (%) for **11**, $C_{42}H_{48}MnN_6$ (691.8): C 72.92, H 6.99, N 12.15; found C 73.01, H 6.89, N 12.25.

Synthesis of [(Et_6N_4)Mn(Cl)] (14): A solution of **8** (2.08 g, 3.43 mmol) in benzene (100 mL) was treated with an excess of iodobenzene dichloride (0.99 g, 3.60 mmol). The color turned immediately from orange to red. The solution was stirred overnight at room temperature. Benzene was evaporated from the reaction mixture, and the remaining dark brown residue was collected with *n*-hexane (80 mL), yielding a green powder (1.34 g, 69 %). Recrystallization from benzene/*n*-hexane gave crystals that were suitable for X-ray analysis. IR (nujol): $\tilde{\nu}_{max}$ = 1595.2 (s), 1522.2 (w), 1488.9 (m), 1465.8 (s), 1378.6 (s), 1316.7 (m), 1294.0 (m), 1266.7 (m), 1238.6 (s), 1076.6 (s), 1016.0 (s), 845.9 (m), 767.7 (m), 721.4 (m) cm^{-1}; UV/Vis (C_6H_6): λ_{max} (ε) = 494 nm, 53 700 $mol^{-1} dm^3 cm^{-1}$); elemental analysis calcd (%) for **14**, $C_{32}H_{38}MnN_4Cl$ (569.1): C 67.54, H 6.73, N 9.85; found C 67.33, H 6.66, N 9.75.

X-ray crystallography of complexes 5, 8, 9, 10, 11, 14: Data concerning crystals, data collection, and structure refinement are listed in Table 1. Diffraction data were collected at 143 K on different devices: mar345 Imaging Plate Detector (**8**, **9**, and **14**), Kuma diffractometer with kappa geometry and equipped with a Sapphire CCD detector (**5**), Rigaku AFC7S diffractometer equipped with a Mercury CCD (**10** and **11**). Data reduction was performed, respectively, with marHKL release 1.9.1,[34] CrysAlis RED 1.6.6[35] and Crystal Clear 1.2.2.[36] Absorption correction[37] was applied to two data sets (**10** and **11**). Structure solutions were determined with ab initio direct methods.[38] All structures were refined using the full-matrix least-squares on F^2 with all non-H atoms anisotropically defined. H atoms were placed in calculated positions using the riding model with $U_{iso} = a \times U_{eq}(C)$ (where *a* is 1.5 for methyl hydrogens and 1.2 for others, while C is the parent carbon atom). The refinement of the data set of **5** could only be achieved by assuming disorder shown by three ethyl chains. This problem was solved by splitting the terminal atoms of these chains (C22, C26, and C32) into two positions (A and B) having the following occupancy factors for site A: 0.584(10) for C22 and 0.488(7) for C26 and C32, and by applying some geometrical restraints. Structure refinement, drawings, and geometrical calculation were carried out on all structures with the SHELXTL software package, release 5.1.[39] Crystallographic data (excluding structure factors) for the structures reported in this paper have been deposited with the Cambridge Crystallographic Data Centre as supplementary publications no. CCDC-154086 for **5**, CCDC-154087 for **8**, CCDC-154088 for **9**, CCDC-154089 for **10**, CCDC-154090 for **11**, CCDC-154091 for **14**, and CCDC-154092 for **7**. Copies of the data can be obtained free of charge on application to CCDC, 12 Union Road, Cambridge CB2 1EZ, UK (fax: (+44) 1223-336-033; e-mail: deposit@ ccdc.cam.ac.uk).

Acknowledgements

We thank the "Fonds National Suisse de la Recherche Scientifique" (Bern, Switzerland, Grant No. 20-61′246.00) and Fondation Herbette (University of Lausanne, N. Re) for financial support.

[1] a) D. Mauzerall, S. Granick, *J. Biol. Chem.* **1958**, *232*, 1141; b) R. B. Woodward, *Angew. Chem.* **1960**, *72*, 651; c) A. Treibs, H. Häberle, *Justus Liebigs Ann. Chem.* **1968**, *718*, 183; d) D. Dolphin, *J. Heterocycl. Chem.* **1970**, *7*, 275; e) F.-P. Montforts, B. Gerlach, F. Höper, *Chem. Rev.* **1994**, *94*, 327–347.

[2] For related earlier work on peripheral functionalization of porphyrinogen and hexahydroporphyrins close to naturally occurring systems, see the contribution from Eschenmoser's group: a) J. E. Johansen, V. Piermattie, C. Angst, E. Diener, C. Kratky, A. Eschenmoser, *Angew. Chem.* **1981**, *93*, 273–275; *Angew. Chem. Int. Ed. Engl.* **1981**, *20*, 261–263; b) R. Waditschatka, E. Diener, A. Eschenmoser, *Angew. Chem.* **1983**, *95*, 641–642; Angew. *Chem. Int. Ed. Engl.* **1983**, *22*, 631–632; c) R. Waditschatka, A. Eschenmoser, *Angew. Chem.* **1983**, *95*, 639–640; *Angew. Chem. Int. Ed. Engl.* **1983**, *22*, 630–631; d) R. Waditschatka, C. Angst, J. E. Johansen, J. C. Plaquevent, J. Schreiber, A. Eschenmoser, *Helv. Chim. Acta* **1985**, *68*, 1312–1337; e) C. Angst, M. Kajiwara, E. Zass, A. Eschenmoser, *Angew. Chem.* **1980**, *92*, 139–140; *Angew. Chem. Int. Ed. Engl.* **1980**, *19*, 140–141.

[3] a) A. Botulinski, J. W. Buchler, M. Wicholas, *Inorg. Chem.* **1987**, *26*, 1540; b) J. W. Buchler, L. Puppe, *Justus Liebigs Ann. Chem.* **1970**, *740*, 142; c) J. W. Buchler, K. L. Lay, P. D. Smith, W. R. Scheidt, G. A. Ruppzecht, J. E. Kenny, *J. Organomet. Chem.* **1976**, *110*, 109; d) J. W. Buchler, C. Dreher, K. L. Lay, Y. J. A. Lee, W. R. Scheidt, *Inorg. Chem.* **1983**, *22*, 888; e) J. W. Buchler, K. L. Lay, Y. J. A. Lee, W. R. Scheidt, *Angew. Chem.* **1982**, *94*, 456; *Angew. Chem. Int. Ed. Engl.* **1982**, *21*, 432; f) P. N. Dwyer, J. W. Buchler, W. R. Scheidt, *J. Am. Chem. Soc.* **1974**, *96*, 2789; g) D. Mauzerall, *J. Am. Chem. Soc.* **1962**, *84*, 2437; h) M. W. Renner, W. Buchler, *J. Phys. Chem*. **1995**, *99*, 8045; i) P. N. Dwyer, L. Puppe, J. W. Buchler, W. R. Scheidt, *Inorg. Chem.* **1975**, *14*, 1782–1785; j) A. Botulinski, J. W. Buchler, Y. J. A. Lee, W. R. Scheidt, *Inorg. Chem.* **1988**, *27*, 927–933; k) A. Botulinski, J. W. Buchler, B. Tonn, M. Wicholas, *Inorg. Chem.* **1985**, *24*, 3239–3245.

[4] L. Bonomo, E. Solari, R. Scopelliti, C. Floriani, N. Re, *J. Am. Chem. Soc.* **2000**, *122*, 5312–5326.

[5] J. F. Kirner, C. A. Reed, W. R. Scheidt, *J. Am. Chem. Soc.* **1977**, *99*, 2557.

[6] a) H. Scheer, H. H. Inhoffen, in *The Porphyrins, Vol. II* (Ed.: D. Dolphin), Academic Press, New York, **1978**, p. 45 and references therein; b) B. Tonn, Ph.D. thesis, Rheinisch-Westfälische Technische Hochschule, Aachen, Germany, **1979**; c) J. W. Buchler, L. Puppe, *Liebigs Ann. Chem.* **1974**, 1046.

[7] M. Gouterman, in *The Porphyrins, Vol. III* (Ed.: D. Dolphin) Academic Press, New York, **1978**, Chapter 1.

[8] a) J. F. Kirner, W. R. Scheidt, *J. Am. Chem. Soc.* **1975**, *14*, 2081; b) R. Mason, G. A. Williams, *J. Chem. Soc. Dalton Trans.* **1979**, 677.

[9] a) O. Kahn, *Molecular Magnetism*, VCH, New York, **1993**; b) R. L. Carlin, *Magnetochemistry*, Springer, Berlin, **1986**; c) C. J. O'Connor, *Prog. Inorg. Chem.* **1982**, *29*, 203.

[10] C. G. Barraclough, R. L. Martin, S. Mitra, R. C. Sherwood, *J. Chem. Phys.* **1970**, *53*, 1643.

[11] P. W. D. Boyd, D. A. Buckingham, R. F. McMeeking, S. Mitra, *Inorg. Chem.* **1979**, *18*, 3585.

[12] C. Da Silva, L. Bonomo, E. Solari, R. Scopelliti, C. Floriani, N. Re, *Chem. Eur. J.* **2000**, *6*, 4518–4531.

[13] A. T. Casey, S. Mitra, in *Theory and Applications of Molecular Paramagnetism* (Eds.: E. A. Boudreaux, L. N. Mulay), John Wiley & Sons, New York, **1976**, pp. 135–255.

[14] a) C. G. Barraclough, R. L. Martin, S. Mitra, R. C. Sherwood, *J. Chem. Phys.* **1970**, *53*, 1639; b) C. G. Barraclough, A. K. Gregson, S. Mitra, *J. Chem. Phys.* **1974**, *60*, 962.

[15] a) A. Ghosh, *Acc. Chem. Res.* **1998**, *31*, 189; b) P. M. Kozlowski, T. G. Spiro, A. Bercés, M. Z. Zgierski, *J. Phys. Chem. B* **1998**, *102*, 2603.
[16] J. L. Hoard, *Ann. N.Y. Acad. Sci.* **1973**, *206*, 18.
[17] W. R. Scheidt, in *The Porphyrin Handbook, Vol. 3* (Eds.: K. M. Kadish, K. M. Smith, R. Guilard), Academic Press, San Diego (CA), **2000**, p. 49.
[18] J. P. Collman, J. L. Hoard, M. Kim, G. Lang, G. A. Reed, *J. Am. Chem. Soc*. **1975**, *97*, 2676.
[19] S. H. Strauss, M. E. Silver, K. M. Long, R. G. Thompson, R. A. Hudgens, K. Spartalian, J. A. Ibers, *J. Am. Chem. Soc.* **1985**, *107*, 4207.
[20] P. Madura, W. R. Scheidt, *Inorg. Chem.* **1976**, *15*, 3182.
[21] W. R. Scheidt, I. Turowska-Tyrk, *Inorg. Chem.* **1994**, *33*, 1314.
[22] W. Jentzen, E. Unger, X.-Z. Song, S.-L. Jia, I. Turowska-Tyrk, R. Schweitzer-Stenner, W. Dreybrodt, W. R. Scheidt, J. A. Shelnutt, *J. Phys. Chem. A* **1997**, *101*, 5789.
[23] T. D. Brennan, W. R. Scheidt, J. A. Shelnutt, *J. Am. Chem. Soc.* **1988**, *110*, 3919.
[24] E. B. Fleischer, C. K. Miller, L. E. Webb, *J. Am. Chem. Soc.* **1964**, *86*, 2342.
[25] R. Pak, W. R. Scheidt, *Acta Crystallogr. Sect. C* **1991**, *47*, 431.
[26] W. R. Scheidt, in *The Porphyrin Handbook, Vol. 7* (Eds.: K. M. Kadish, K. M. Smith, R. Guilard), Academic Press, San Diego (CA), **2000**, p. 1.
[27] L. N. Mulay, in *Theory and Applications of Molecular Paramagnetism* (Eds.: E. A. Boudreaux, L. N. Mulay), John Wiley & Sons, New York, **1976**, pp. 491 – 495.
[28] a) E. J. Baerends, D. E. Ellis, P. Ros, *Chem. Phys.* **1973**, *2*, 42; b) E. J. Baerends, P. Ros, *Chem. Phys.* **1973**, *2*, 51; c) E. J. Baerends, P. Ros, *Chem. Phys.* **1975**, *8*, 41; d) E. J. Baerends, P. Ros, *Int. J. Quantum Chem.* **1978**, *S12*, 169; e) P. M. Boerrigter, G. te Velde, E. J. Baerends, *Int. J. Quantum Chem.* **1988**, *33*, 87; f) G. te Velde, E. J. Baerends, *J. Comput. Phys.* **1992**, *99*, 84; g) T. Ziegler, V. Tschinke, E. J. Baerends, J. G. Snijders, W. Ravenek, *J. Phys. Chem.* **1989**, *93*, 3050.
[29] S. H. Vosko, L. Wilk, M. Nusair, *Can. J. Phys.* **1980**, *58*, 1200.
[30] A. D. Becke, *Phys. Rev.* **1988**, *A38*, 2398.
[31] J. P. Perdew, *Phys. Rev.* **1986**, *B33*, 8822.
[32] L. Versluis, T. Ziegler, *J. Chem. Phys.* **1988**, *88*, 322.
[33] E. Solari, F. Musso, E. Gallo, C. Floriani, N. Re, A. Chiesi-Villa, C. Rizzoli, *Organometallics* **1995**, *14*, 2265 – 2276.
[34] Z. Otwinowski, W. Minor, *Methods in Enzymology, Vol. 276: Macromolecular Crystallography, Part A* (Eds.: C. W. Carter, Jr., R. M. Sweet), Academic Press, New York, **1997**, 307 – 326.
[35] Kuma Diffraction Instruments Gmbh, PSE-EPFL module 3.4, Lausanne, Switzerland, **2000**.
[36] J. W. Pflugrath, *Acta Crystallogr. Sect. D* **1999**, *55*, 1718.
[37] TeXsan for Windows 1.0.6 and REQAB 4 1.1, Molecular Structure Corporation, New Trails Drive, The Woodlands, Texas 77381-5209 (USA), **1997 – 1999**.
[38] G. M. Sheldrick, *Acta Crystallogr.* **1990**, *A46*, 467.
[39] Bruker AXS, Madison, Wisconsin 53719 (USA), **1997**.

Received: December 11, 2000 [F2929]

 © WILEY-VCH Verlag GmbH, D-69451 Weinheim, 2001 0947-6539/01/0712-2546 $ 17.50+.50/0